Impact of the nonstationarity of a supercritical perpendicular collisionless shock on the dynamics and the energy spectra of pickup ions

Z. W. Yang, Bertrand Lembège, Q. M. Lu

Impact of the nonstationarity of a supercritical perpendicular collisionless shock on the dynamics and energy spectra of pickup ions

Z. W. Yang,[1,2] B. Lembège,[1] and Q. M. Lu[2]

Received 8 December 2010; revised 23 March 2011; accepted 9 May 2011; published 11 August 2011.

[1] Both hybrid and full particle simulations and recent experimental results have clearly evidenced that the front of a supercritical quasi-perpendicular shock can be nonstationary. One proposed mechanism responsible for this nonstationarity is the self-reformation of the shock front being due to the accumulation of reflected ions. On the other hand, a large number of studies have been made on the acceleration and heating of pickup ions (PIs) but most have been restricted to a stationary shock profile only. Herein, one-dimensional test particle simulations based on shock profiles issued from one-dimensional particle-in-cell simulation are performed in order to investigate the impact of the shock front nonstationarity (self-reformation) on the acceleration processes and the resulting energy spectra of PIs (protons H^+) at a strictly perpendicular shock. PIs are represented by different shell distributions (variation of the shell velocity radius). The contribution of shock drift acceleration (SDA), shock surfing acceleration (SSA), and directly transmitted (DT) PI's components to the total energy spectra is analyzed. Present results show that (1) both SDA and SSA mechanisms can apply as preacceleration mechanisms for PIs, but their relative energization efficiency strongly differs; (2) SDA and SSA always work together at nonstationary shocks (equivalent to time-varying shock profiles) but SDA, and not SSA, is shown to dominate the formation of high-energy PIs in most cases; (3) the front nonstationarity reinforces the formation of SDA and SSA PIs in the sense that it increases both their maximum energy and their relative density, independently on the radius of PI's shell velocity; and (4) for high shell velocity around the shock velocity, the middle energy range of the total energy spectrum follows a power law $E_k^{-1.5}$. This power law is supported by both SDA and DT ions (within two separate contributing energy ranges) for a stationary shock and mainly by SDA ions for a nonstationary shock. In both cases, the contribution of SSA ions is comparatively weak.

Citation: Yang, Z. W., B. Lembège, and Q. M. Lu (2011), Impact of the nonstationarity of a supercritical perpendicular collisionless shock on the dynamics and energy spectra of pickup ions, *J. Geophys. Res.*, *116*, A08216, doi:10.1029/2010JA016360.

1. Introduction

[2] The physics of collisionless shocks is a very broad topic in space and astrophysical plasmas. Shocks are of great interest since, within the shock transition, the bulk energy of the plasma is converted irreversibly into thermal energy [*Tidmann and Krall*, 1971; *Tsurutani and Stone*, 1985; *Lembège*, 1989; *Lembège et al.*, 2004]. The particular difficulty consists in identifying the main physical mechanisms responsible for this energy conversion and the resulting particle energization. One important application is concerning the formation of energetic pickup ions (PIs). It is well known that the shell radii of PIs are different for various types of shocks met in space plasmas as illustrated in Figure 1 [*Lee et al.*, 1996]. Figure 1a corresponds to a cometary shock and shows that the ions picked up further from the comet nucleus, where the ionization rate is smaller, have been compressed and energized in the decelerating mass-loaded flow, whereas the greater number of ions near the bow shock are picked up by a slower wind due to the mass loading. Figure 1b shows for the termination shock (TS), that interplanetary ionized ions picked up in the inner heliosphere have been cooled in the divergent solar wind. Those pickup ions (PIs) form a thick shell with radii varying from small to large values in velocity space [*Vasyliunas and Siscoe*, 1976]. Figure 1c shows for the corotating interaction region (CIR) shocks, that the interplanetary ions picked up further from the shock have also been cooled but by a lesser amount in the inner

[1]LATMOS-UVSQ-IPSL-CNRS, Guyancourt, France.
[2]CAS Key Laboratory of Basic Plasma Physics, School of Earth and Space Sciences, University of Science and Technology of China, Hefei, China.

0148-0227/11/2010JA016360

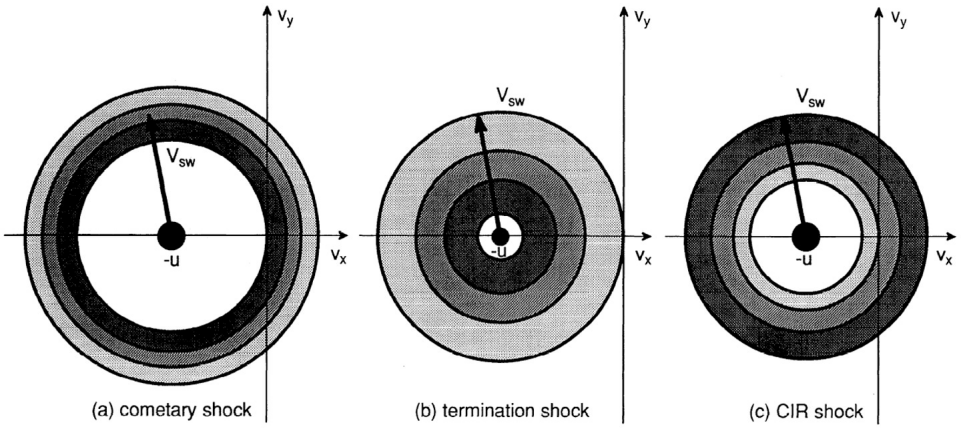

Figure 1. PIs and solar wind velocity space distributions in the plane ($v_z = 0$) incident on (a) cometary, (b) termination, and (c) CIR shocks. The distributions are in the shock frame in which the solar wind (dark circle) is normally incident with speed u. The pickup ion distributions are spherically symmetric about the solar wind with speeds of order V_{sw} in the solar wind frame [from *Lee et al.*, 1996].

heliosphere. Those PIs form a thick velocity shell distribution with radii ($\tilde{V}_{shell}$) varying from middle to large values. In summary, analyzing the processes responsible for PI's energization requires to investigate the effect of $\tilde{V}_{shell}$ variation on PI's dynamics (and if possible within a self-consistent approach).

[3] An important number of works has been already dedicated to the mechanisms responsible for the formation of PIs. The theory of diffusive shock acceleration (DSA) [*Axford et al.*, 1977; *Bell*, 1978a, 1978b; *Krymsky*, 1977; *Blandford and Ostriker*, 1978; *Lee*, 1983; *Blandford and Eichler*, 1987; *Webb et al.*, 1995; *Malkov and Drury*, 2001; *Li et al.*, 2003; *Giacalone*, 2004; *Zank et al.*, 2006] is believed to be the most important mechanism of shock acceleration for quasi-parallel shocks. However, a similar theory does not work efficiently at low energies at quasi-perpendicular shocks (e.g., the heliospheric termination shock), where the reflected ions return to the shocks almost immediately due to their gyromotion in the upstream magnetic field. Therefore, shock drift acceleration (SDA) [*Hudson*, 1965; *Webb et al.*, 1983; *Decker and Vlahos*, 1985; *Decker*, 1988; *Begelman and Kirk*, 1990; *Chalov*, 2001] and shock surfing acceleration (SSA) [*Sagdeev*, 1966; *Katsouleas and Dawson*, 1983; *Zank et al.*, 1996; *Lee et al.*, 1996; *Lee*, 1999; *Shapiro and Ucer*, 2003] are considered to play important roles in ion acceleration or preacceleration at quasi-perpendicular shocks. Indeed, a two steps scenario has been proposed: a first preacceleration step where the SSA is invoked to accelerate ions to an energy high enough to reach the threshold above which, second, the DSA process may efficiently apply. However, the relative contribution of each primary acceleration mechanism (SSA and SDA) to the total energy spectrum of PIs within a self-consistent shock approach has not been analyzed yet.

[4] Previous laboratory experiments [*Morse et al.*, 1972], space observations [*Lobzin et al.*, 2007; *Mazelle et al.*, 2009], particle-in-cell (PIC) simulations [*Biskamp and Welter*, 1972; *Lembège and Dawson*, 1987; *Lembège and Savoini*, 1992; *Shimada and Hoshino*, 2000; *Schmitz et al.*, 2002; *Scholer et al.*, 2003; *Nishimura et al.*, 2003; *Lee et al.*, 2004, 2005a], and hybrid simulations [*Hellinger et al.*, 2002; *Lembège et al.*, 2009] have revealed that high Mach number, quasi-perpendicular collisionless shocks are nonstationary for relative low β_i case [*Hada et al.*, 2003]. One mechanism proposed for this nonstationarity is the cyclic self reformation due to the reflected ions which accumulate at a foot distance from the ramp. The foot increases in time until reaching an amplitude comparable to that of the ramp. Then, a new ramp builds up and starts reflecting a new set of upstream ions. This cyclic process appears to be quite robust since observed for strictly perpendicular shocks and within quasi-perpendicular propagation range, for 1-D/2-D PIC [*Lembège and Savoini*, 1992] as well as in hybrid simulations [*Hellinger et al.*, 2002]. More recently, *Lembège et al.* [2009] and *Hellinger et al.* [2007] have evidenced two different nonstationary dynamics of perpendicular shocks defined according to the orientation of the upstream magnetic field. When the magnetic field is inside the 2-D simulation plane, large amplitude whistler waves are emitted from the front, stay in phase with it and strongly interact with reflected ions so that the self-reformation is inhibited. This waves emission takes place above a certain Mach threshold below which the self-reformation alone is observed. In contrast, as the magnetic field is outside the 2-D simulation plane, no whistler waves emission is evidenced, no scattering of reflected ions takes place and only self-reformation is recovered. The transition between two cases (with magnetic field in and out the simulation plane) requires the use of large scale full 3-D PIC simulations which have been recently performed by *Shinohara et al.* [2011] using a realistic mass ratio and who evidenced the following points: (1) in contrast with previous 2-D results, the self-reformation and whistler emission coexist in 3-D simulation; and (2) the amplitude of the observed whistler emission in the 3-D case is smaller than that of the 2-D result; this result can be purely caused by 3-D effects. Moreover, several other 1-D PIC simulations have shown that, for strictly perpendicular shocks, the self-reformation persists for a realistic mass ratio and high ω_{pe}/Ω_{ce} ratio [*Scholer et al.*, 2003] and is still controlled by the accumulation of reflected ions even

in presence of microinstabilities within the foot region [*Muschietti and Lembège*, 2006]. Extensively, for oblique (quasi-perpendicular) 1-D shocks and a realistic mass ratio, the self-reformation is again present but becomes controlled by the modified two-stream instability between the reflected ions and the incoming electrons [*Scholer and Matsukiyo*, 2004]. Since the self-reformation is a robust process, we choose to focus our attention in the present analysis on the impact of a self-reforming shock, in the most simple conditions, i.e., for a strictly perpendicular 1-D shock and low mass ratio (no pollution by oblique whistler waves or presence of microinstabilities), on the dynamics of PIs.

[5] *Yang et al.* [2009] have already investigated the ion acceleration at such self-reforming supercritical perpendicular shocks. Their studies have been focused on the impact of this shock front nonstationarity on SDA and SSA mechanisms, and their consequence on individual protons trajectory (introduced as upstream Maxwellian and shell distributions) and on their statistical behavior. However, the impact of shock front reformation on the particle spectrum has not been analyzed yet. This gave us the motivation for investigating the impact of shock front nonstationarity on PI's energy spectra and on the relative contribution of SSA and SDA ions to this spectrum.

[6] This paper represents an extension of a previous work [*Yang et al.*, 2009]. Herein, we use similar test particle calculations based on fields of shock profiles issued from one-dimensional PIC simulation (where nonstationary effects are self-consistently included) in order to address the following questions: (1) What is the impact of the shell radius variation on the occurrence and energization of SSA, SDA and DT ions? (2) How these SSA, SDA and DT ions compete each other in particular on their respective contribution to the total energy spectra? (3) What's the impact of the shock front self-reformation on this competition?

[7] We note that in our model the test particle simulation of PIs is not fully self-consistent. The pickup ion scale shock structures, which may be important especially at heliospheric termination shock due to the highly relative density of pickup protons [*Liewer et al.*, 1993; *Lee et al.*, 2005b; *Matsukiyo et al.*, 2007; *Wu et al.*, 2009; *Zank et al.*, 2010], are neglected here. Our present approach results from a compromise based on the results by *Vasyliunas and Siscoe* [1976] which indicate that the percentage of pickup protons to solar wind protons at 50AU is estimated to be 10% and increases linearly with distance from the sun; Then, the shock front microstructures of the CIR-associated shocks or CME-driven shocks at a few tens of AU away from the sun and their nonstationarity are self-consistently present and mainly driven by protons. In addition, our approach is also supported by the results from *Chapman et al.* [2005] and *Lee et al.* [2005b], who have investigated the impact of upstream PIs (10% with shell radius $V_{shell} = 25V_{thp}$ where V_{thp} is the thermal velocity of solar wind protons) on the self-reformation process. The authors have shown that (1) the addition of 10% PIs does not modify the solar wind proton phase space and the dynamics of the self-reforming shock which is unchanged, (2) background protons dynamics proceeds essentially as in the absence of PIs, and (3) a subset of PIs reflect off the shock to form a weak and extended foot region which stands upstream of the shock and is quasi-stationary. However, the authors did not provide information on the relative contribution of SDA and SSA ions (both from PIs and solar wind protons) and their contribution in the resulting energy spectra. Our present simulations apply to the cases of relatively low percentage of heavy ions where self-reformation is not affected by the presence of PIs and is mainly driven by the solar wind protons. Furthermore, our approach presents the advantage of relative simplicity, of low computer cost and allows us to perform a detailed parametric analysis and high statistical study necessary for computing the energy spectra for PIs with different velocity shells.

[8] This paper is organized as follows: In section 2, we briefly describe the numerical model used herein. Sections 3 and 4 present the simulation results at (1) fixed shock profiles and (2) time-evolving shock profiles, respectively. In section 5, we also discuss and compare our results with previous works. The main conclusions will be summarized in section 5.

2. Conditions of Numerical Simulations

[9] Investigating PI's acceleration in the vicinity of a nonstationary shock requires a spatial range large enough for particles to do gyromotion before and after the shock, and a spatial resolution small enough to include the detailed physics for shock front microstructure varying during the self-reformation. We implement a combination of a 1-D PIC simulation to model the fields and a test particle simulation to follow the orbits of a large number of energetic PIs. First, we perform a one-dimensional PIC simulation similar to previous work [*Lembège and Dawson*, 1987; *Lembège and Savoini*, 1992; *Hada et al.*, 2003], where the shock is initiated by a magnetic piston (applied current pulse). Therefore, the shock geometry is defined in the upstream frame: the shock propagates along the $\tilde{x}$ direction and an upstream magnetic field $\tilde{B}_o$ is applied along the $\tilde{z}$ axis. All dimensionless quantities are indicated by a tilde "~" and are normalized as follows. The spatial coordinate is $\tilde{x} = x/\Delta$; velocity $\tilde{v} = v/\omega_{pe}\Delta$; time $\tilde{t} = \omega_{pe}t$, electric field $\tilde{E} = eE/m_e\omega_{pe}^2\Delta$; magnetic field $\tilde{B} = eB/m_e\omega_{pe}^2\Delta$. The parameters Δ, ω_{pe}, m_e and e are the numerical grid size, the electron plasma frequency, the electron mass, and the electric charge, respectively. The plasma conditions are similar to those used by *Hada et al.* [2003] and *Yang et al.* [2009]. All basic parameters are summarized as follows: the size of the plasma simulation box $\tilde{L}_x = 4096$; velocity of light $\tilde{c} = 3$, and mass ratio of proton and electron $m_i/m_e = 84$. In order to achieve reasonable run times and simulation domains a ratio of $\tilde{\omega}_{pe}/\tilde{\Omega}_{ce} = 2$ had to be used as by *Matsukiyo et al.* [2007]. Initially, the particle density is in each grid $n_i = n_e = 50$. The electron/ion temperature ratio is $T_e/T_i = 1.58$. The ambient magnetic field is $|\tilde{B}_o| = 1.5$. The shock has an averaged Alfvénic Mach number, $M_A = V_{shock}/V_A = 5.2$ where the upstream Alfvén velocity $\tilde{V}_A$ is equal to 0.16; the averaged V_{shock} value is measured over several cyclic self-reformations. For these initial conditions, the upstream plasma parameters are summarized in Table 1 for both electrons and protons.

[10] Second, we follow the full motion of test particle PIs interacting with the electromagnetic fields of a shock profile issued from the above PIC simulation. In order to analyze the impact of a varying $\tilde{V}_{shell}$, shell distributions of PIs are released with different shell radii from $\tilde{V}_{shell} = 5\tilde{V}_{thix,y,z}$ to $48\tilde{V}_{thix,y,z}$, where $\tilde{V}_{thix,y,z}$ is the proton thermal speed in our

Table 1. Upstream Plasma Parameters Defined for the PIC Simulation

	Electrons	Ions
Thermal velocity ($\tilde{V}_{thx,y,z}$)	0.2	0.017
Debye length ($\tilde{\lambda}_D$)	0.2	0.16
Larmor gyroradius ($\tilde{\rho}_c$)	0.4	2.91
Inertia length ($\tilde{c}/\tilde{\omega}_p$)	3.0	27.5
Gyrofrequency ($\tilde{\Omega}_c$)	0.5	0.006
Plasma frequency ($\tilde{\omega}_p$)	1.0	0.11
Gyroperiod ($\tilde{\tau}_c$)	12.55	1055.46
Plasma beta ($\tilde{\beta}$)	0.0355	0.0225

PIC simulation; note that the value 48 $\tilde{V}_{thix,y,z}$ almost corresponds to the shock velocity. We will consider pickup protons (H^+) only. Those test particles (50 particles per cell) are initially distributed far upstream (at 100 grid cells away from the ramp). Our test particle simulation can be separated into three parts. In the first part (fixed shock profiles), we choose three typical shock profiles at three different times within one self-reformation cycle, and we analyze separately the PI's spectra at these shock profiles. Herein, the propagating shock is injected with a velocity equals to that measured in the PIC simulation; its instantaneous Mach number can differ from the average value M_A = 5.2 (section 3). In the second part (time-varying shock profiles), we will investigate the spectra of PIs interacting with a continuously time-evolving shock, while the shock is self-reforming (section 4.2). The simulation time covers about five successive reformation cycles of the shock front.

3. Dynamics of PIs in Fixed Shock Profiles

[11] The time evolution of the perpendicular shock is shown in Figure 2a, which plots the main magnetic component $\tilde{B}_z$ issued from the 1-D PIC simulation (different colors correspond to different reformation cycles). The shock is in supercritical regime characterized by noticeable foot, ramp and overshoot, and its front is nonstationary (self-reformation). As the shock propagates, more and more ions are reflected by the ramp and accumulate in the foot with a percentage relatively high so that the foot amplitude increases and reaches a noticeable value (~ the half of the "old" ramp). Then, a "new" shock ramp builds up and starts reflecting new incoming ions. The foot amplitude still increases and a "new" shock front is well formed. Simultaneously, the previous ("old") shock front becomes weaker and weaker and stays located downstream of the "new" front. The self-reformation is characterized by a cyclic period about $1.73\Omega_{ci}^{-1}$ (= 0.28 T_{ci}), where T_{ci} is the upstream ion gyroperiod. During this self reformation, not only the amplitude of the overshoot and the foot varies relatively, but also the spatial scales of the ramp and the foot do.

[12] In order to investigate the dynamics and energy spectrum of PIs in different shock profiles, three typical shock profiles (I, II and III) are selected within one self-

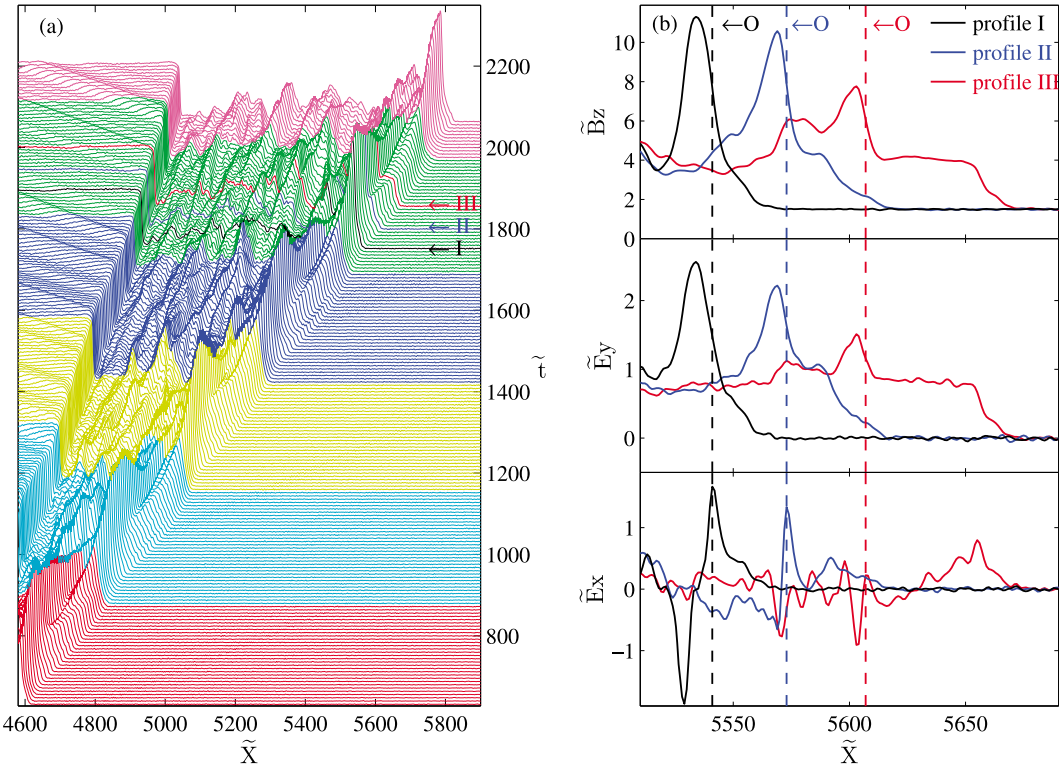

Figure 2. (a) Stackplot of the main magnetic field $\tilde{B}_z$ versus $\tilde{X}$ at a nonstationary (self-reforming) shock. (b) Three shock profiles I (black), II (blue), and III (red) selected at $\tilde{t}$ = 1752, 1800, and 1856 of the main magnetic field $\tilde{B}_z$ and electric fields $\tilde{E}_y$ and $\tilde{E}_x$. The selected times are indicated by arrows within the fifth reformation cycle (corresponding to the green stackplot of Figure 2a). Vertical dashed lines denote the old ("O") ramp locations at these three different shock profiles.

reformation cycle (from $\tilde{t}$ = 1692 to 1968, i.e., the 5th cycle) and are shown in Figure 2b. Profiles I, II and III represent the snapshots of $\tilde{B}_z$, $\tilde{E}_y$ and $\tilde{E}_x$ at $\tilde{t}$= 1752, 1800 and 1856, respectively. In profile I, the shock overshoot and the cross-shock potential (or $\tilde{E}_x$ field) at the ramp almost reach their maximum. The ramp, denoted by "O" (as "old"), is quite steep. In profile II, the shock front includes the ramp "O" and a noticeable foot amplitude which is about one third of the overshoot. In profile III, the amplitude of the old ramp "O" has strongly decreased. Simultaneously, the foot amplitude reached the half of that of the overshoot and become much broader than before. The ramps "O" of profiles I, II and III are at $\tilde{X}$ = 5541, 5573, and 5607, respectively, and their corresponding measured "instantaneous" velocities are $3.9\tilde{V}_A$, $4.69\tilde{V}_A$ and $5.08\tilde{V}_A$. Their shock front widths (including foot and ramp) are about $1.2\tilde{c}/\tilde{\omega}_{pi}$, $1.7\tilde{c}/\tilde{\omega}_{pi}$ and $2.4\tilde{c}/\tilde{\omega}_{pi}$, and are measured from the upstream edge of the foot to the peak of the magnetic overshoot; the upstream edge of the foot is defined as the location where the magnetic field has increased by 6.67% over its upstream value [*Burgess et al.*, 1989; *Yang et al.*, 2009].

[13] Figure 3a shows the phase space $\tilde{V}_{ix}$ versus $\tilde{X}_i$ of the PIs with different initial shell radii $\tilde{V}_{shell}$ = 5, 10, 28 and $48\tilde{V}_{thix,y,z}$ from top to bottom in each column, for profile I, II and III, respectively. Corresponding magnetic field $\tilde{B}_z$ and electric field $\tilde{E}_x$ are also shown for reference. Incident ions can be divided into three groups as done by *Yang et al.* [2009]: reflected SDA ions (red dots), reflected SSA ions (green dots) and DT ions together with incoming ions (black dots). More specifically, we first separate the upstream ions into two groups in each case: the reflected (R) ions and directly transmitted (DT) ions. The selected reflected ions must satisfy the following criteria: (1) these are located upstream the ramp, i.e., $\tilde{X}_i > \tilde{X}_{ramp}$; and (2) their velocity $\tilde{V}_{ix}$ must be larger than the shock velocity $\tilde{V}_{shock}$. Second, the R ions can be divided into two subpopulations by using a simple criterium used by *Lever et al.* [2001]: the SDA ions are primarily reflected by the Lorentz force; that is, these verify $\tilde{E}_x < (\tilde{V}_{iy}\tilde{B}_z - \tilde{V}_{iz}\tilde{B}_y)/\tilde{c}$ in the ramp. SDA ions do return upstream once before passing through the shock front. In contrast, the SSA ions are primarily reflected by the electrostatic force; that is, these verify $\tilde{E}_x \geq (\tilde{V}_{iy}\tilde{B}_z - \tilde{V}_{iz}\tilde{B}_y)/\tilde{c}$ in the ramp. When crossing the shock front, DT ions go downstream without any reflection, and only get a bulk velocity downstream. In contrast, reflected ions are accelerated and become the most energetic. Main results are as follows: (1) for small shell cases (first and second rows of Figure 3a), DT ions are invisible in profile I (i.e., all PI's ions are reflected), emerge in profile II, and become noticeable in profile III; the occurrence of DT ions is facilitated for high $\tilde{V}_{shell}$ values; (2) SDA ions are always evidenced whatever are the $\tilde{V}_{shell}$ value and the shock profile; (3) for large shell cases (third and fourth rows of Figure 3a), more SSA particles are evidenced in profile I rather than in profiles II and III; (4) the upstream spatial range where reflected ions extend (both for SDA and SSA PIs when these are evidenced) is large as the shock profile is steepy (profiles I and II), but strongly decreases as the foot amplitude and its width increases (profile III); indeed the fields amplitude at the ramp is lower and the reflection efficiency is weaker; (5) however, this spatial extension range largely increases upstream with $\tilde{V}_{shell}$ whatever the shock profile is. In other words, both the $\tilde{V}_{shell}$ value and the nonstationarity of the shock front play the role of filters in terms of reflection efficiency and of respective formation of SSA and SDA ions: Figure 3b shows the density profiles of each SDA (red), SSA (green), and incoming and DT (black) ion population for each case considered in Figure 3a. These plots clearly evidence several features: for all profiles, SDA PIs strongly accumulate (higher local density) for low $\tilde{V}_{shell}$ over a relatively short foot region which largely expands upstream as $\tilde{V}_{shell}$ increases (lower local density) (Figure 3a). For profiles I and II, the width of this foot is much larger than that due to the background protons only; in contrast, the PI's foot for profile III can be shorter than (Figure 3a, first panel), comparable to (Figure 3a, second panel) or larger than (Figure 3a, third and fourth panels) that of background protons; local SDA PI's density decrease in the downstream region as shell $\tilde{V}_{shell}$ increases. In the case of profile II (steep ramp with an increasing foot), this density drastically decreases just after the ramp (local density of SDA PIs is almost suppressed as shown for profile II in Figure 3b), especially at low energy cases. The downstream distance (from the shock front) over which this decrease takes place increases with $\tilde{V}_{shell}$ since DT PIs succeed to penetrate further downstream.

[14] Corresponding energy spectra of PIs are shown in Figure 4, and are measured from upstream ($\tilde{X}_{ramp}$ + 300) to far downstream ($\tilde{X}_{ramp}$ − 600) in the upstream frame (i.e., our simulation frame where the upstream plasma is at rest). Contributions of each particle components, namely, SDA, SSA, and DT together with incoming ions, are identified separately by red, green, black dots, respectively. The total spectrum (all mixed populations) is represented by a blue solid curve. The peak in the spectrum in each subplot (dark dots and blue curve) indicates the upstream thin shell distribution, and the broadened part around this peak is due to the acceleration of incoming ions within the shock front. Main results are summarized as follows:

[15] 1. For small $\tilde{V}_{shell}$ (first and second panels of Figures 4a–4c), only SDA ions are responsible for the total spectrum in profile I and no SSA ions are formed (except in second panel of Figure 4c); this spectrum is flatter for profile I than for profiles II and III, within the range 2 ~ 100 Mev (i.e., below the density shoulder). Let us note that the dark dots in first and second panels of Figure 4a correspond to the upstream reference spectra, since no DT ions are evidenced in first and second panels (profile I) of Figure 3a. However, for profiles II and III (first and second panels of Figures 4b and 4c), both SDA and DT ions contribute to the most part of the spectrum but the highest energy part is only supported by SDA ions.

[16] 2. For high $\tilde{V}_{shell}$ cases (third and fourth panels of Figure 4a) and for profile I, the density of SSA ions strongly increases and becomes comparable to that of DT ions, but the density of SDA ions is higher than that of the other components by an order of magnitude. In contrast, in profiles II and III (third and fourth panels of Figures 4b and 4c) the density of SDA ions becomes comparable to that of DT ions and the density of SSA becomes lower than that of the other components by an order of magnitude.

[17] 3. For very high $\tilde{V}_{shell}$, profile I (fourth panel of Figure 4a) helps the formation of monoenergetic type spec-

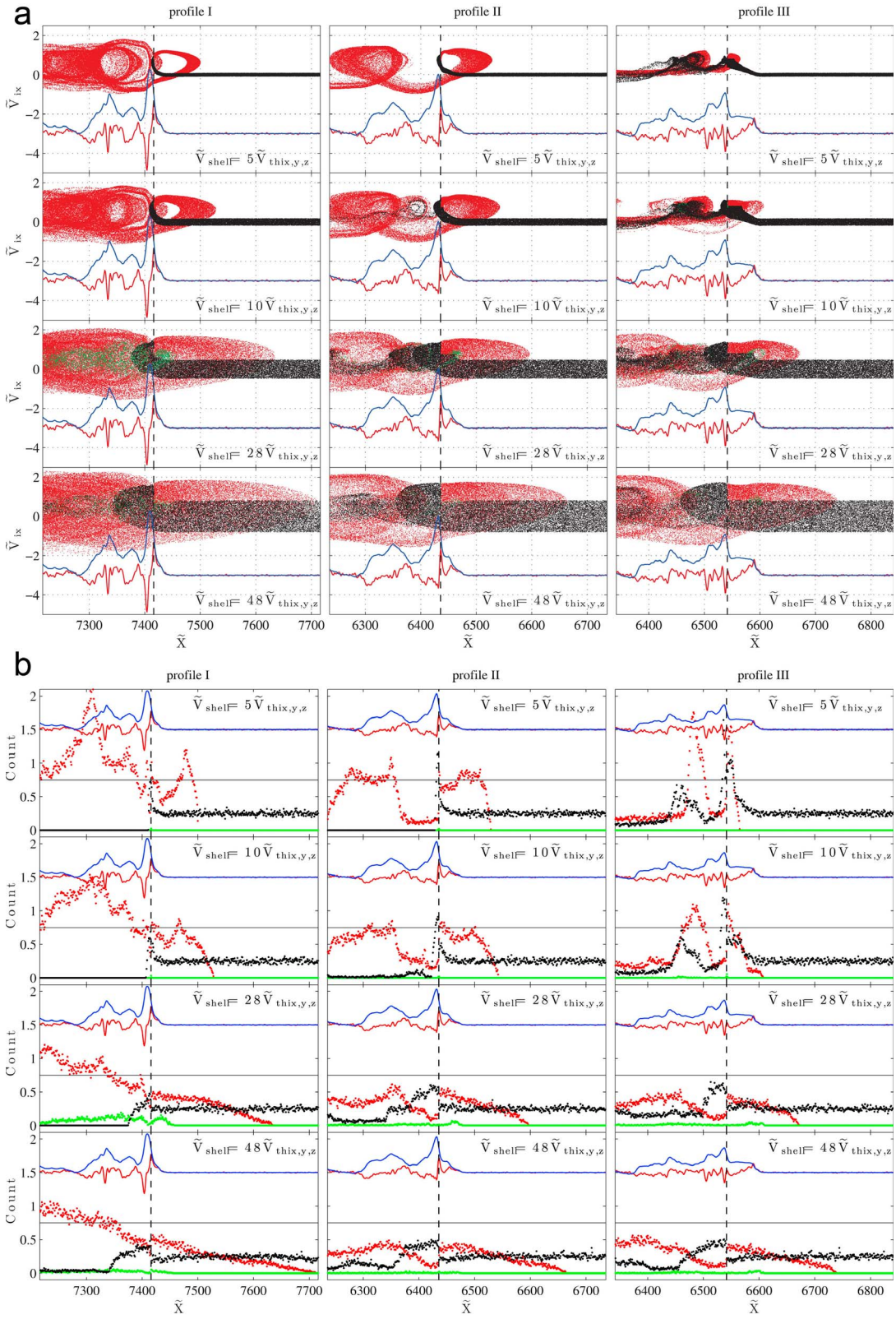

Figure 3. (a) Phase space plots ($\tilde{V}_{ix} - \tilde{X}_i$) of PI's ions (incoming and DT ions (black), SDA reflected ions (red), SSA reflected ions (green)) with different initial shell velocities $\tilde{V}_{shell}$ = 5, 10, 28 and 48$\tilde{V}_{thix,y,z}$ at the three shock profiles I, II, and III selected within the fifth reformation cycle. For reference, shock profiles are also shown in each panel. Vertical dashed lines indicate the old ("O") ramp locations of the different shock profiles. (b) Density profiles of each SDA (red dots), SSA (green dots), and incoming and DT (black dots) ion population for each case considered in Figure 3a.

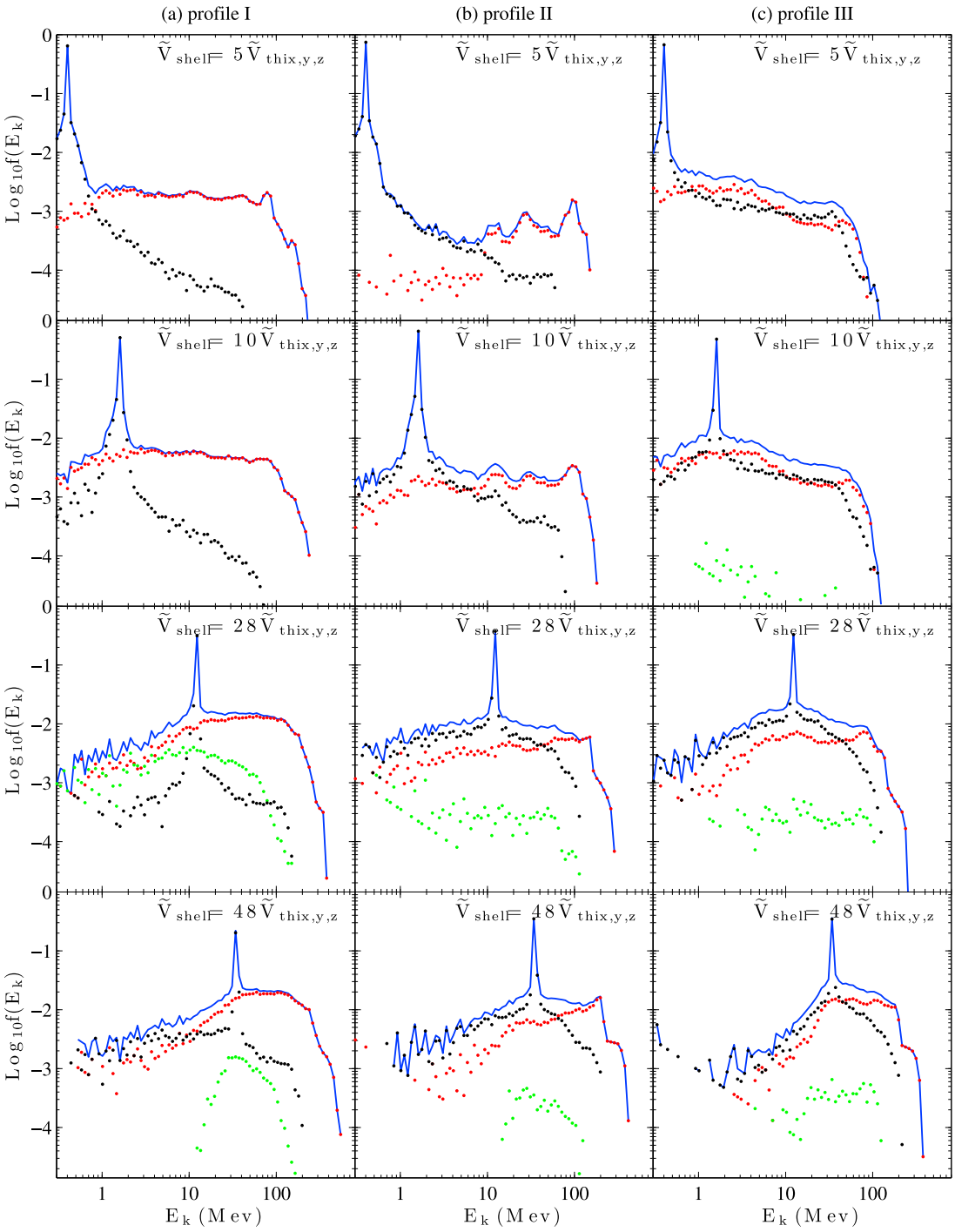

Figure 4. (a–c) Energy spectra of PI's ions corresponding to the cases shown in Figure 3a. Red, green, and black dots indicate the contributions of "SDA," "SSA," and "DT plus incoming" ions to the total spectra (blue solid curve), respectively. The black dots in first and second panels (Figure 4a) correspond to upstream reference spectra since no DT ions are evidenced in Figure 3a (profile I first and second panels).

trum of SSA ions (bump shape centered around $E_k = 40$ Mev); in the other cases, the spectrum of SSA ions (when these can be evidenced) is quite broad.

[18] 4. The SDA ions always dominate in the high energy tail ($E_k > 100$ Mev), whatever are the $\tilde{V}_{shell}$ value and the shock profile.

[19] In summary, the filtering effects previously mentioned (corresponding to $\tilde{V}_{shell}$ variations and to the shock front nonstationarity) play a key role in the relative contribution of the different populations to the total energy spectrum and in their resulting efficiency of ion energization. One important point is that SDA ions, and not SSA ions, always bring a

dominant contribution to the high energy part of the total energy spectrum (cutoff energy shoulder).

4. Dynamics of PIs in Time-Varying Shock Profiles

4.1. Ion Maxwellian Distribution

[20] In this section, we perform a test particles simulation analysis complementary to our previous work [*Yang et al.*, 2009] by investigating in details the energization of SDA and SSA ions interacting with a continuously self-reforming shock profile shown in Figure 2a. We use an incident ion Maxwellian distribution with a thermal velocity $\tilde{V}_{thix,y,z} = 0.017$ identical to that used in our previous PIC simulation. The test particles are initially distributed far upstream away from the shock (from $\tilde{X}_i = 4637$ to $\tilde{X}_i = 6007$ with 50 particles per cell) at a chosen time $\tilde{t} = 628$ of the PIC simulation. At that time, the shock front is well formed and its nonstationarity has already started. We identify each SSA, SDA and DT ion population by using the same method as in our previous paper [*Yang et al.*, 2009]. The method is now improved by using instantaneous shock velocity instead of the time-averaged shock velocity measured at the ramp. Within one self-reformation cycle, the "old" ramp is continuously tracked in time until the "new" ramp is strong enough to reflect new incoming ions.

[21] Let's restrict our attention to the 5th reformation cycle. Figure 5a shows the shock profiles ($\tilde{B}_z$ and $\tilde{E}_x$) and phase space plots ($\tilde{V}_{ix} - \tilde{X}_i$) at the beginning time ($\tilde{t} = 1692$) of the 5th reformation cycle. We have removed the particles which have already encountered the shock ramp (i.e., located already behind the ramp), and begin to count separately the number of reflected (R) ions (i.e., SDA and SSA) and directly transmitted ions at the old ramp (marked by "O") in each time step. Figure 5b shows similar plots in the end of 5th cycle ($\tilde{t} = 1968$). After that time, the 6th reformation cycle starts and the new ramp (marked by "N") begins to reflect new incoming ions. In this panel, all ions which have been reflected by the old ramp are marked by green dots. During this cycle, the count of R and DT ions in each time step at the old ramp are defined by N_R and N_{DT}, respectively. The count of particles nipped between the old ramp and the new ramp are defined as N'_{DT}. Those nipped ions also include DT ions, and they will go downstream without any reflection at later time. Figure 5c shows the percentage of SDA and SSA particles versus time. The percentage for each population at each time step is calculated as: $N\% = N/N_{total} \times 100\%$, where $N_{total} = N_R + N_{DT}$ correspond to the total number of incident ions having interacted with the old ramp during the fifth reformation cycle; N_R and N_{DT} values are measured at the end of the cycle ($\tilde{t} = 1968$). Main results are as follows:

[22] 1. Results again confirm that the density of SSA ions is always much lower that of SDA ions (factor 20);

[23] 2. We found two typical time stages: in the first half stage of the reformation cycle (from $\tilde{t} = 1692$ to $\tilde{t} = 1816$), the old ramp can generate both SDA and SSA ions. In contrast, in the second half stage (from $\tilde{t} = 1816$ to $\tilde{t} = 1968$), there are no newborn SSA particles at the old ramp. The decrease of the cross-shock potential affects more rapidly SSA than SDA ions. SDA percentage keeps in increasing before the cycle ends but starts slightly saturating at late time of the cycle.

[24] 3. The total kinetic energy versus time calculated for each population (Figure 5d) increases for both SSA and SDA ions, respectively, until $\tilde{t} = 1805$ and $\tilde{t} = 1850$, and decreases afterwards. It implies that the energization process itself is finished before the end of the cycle. SDA ions are still formed (Figure 5c) but these are much less energetic. This is due to the decrease of the fields amplitude at the ramp "O" before the new ramp "N" becomes strong enough to start reflecting a new set of upstream ions.

[25] 4. The corresponding average kinetic energy for each population (Figure 5e) shows comparable values for SSA and SDA ions. This statistical average is performed separately with respect to the number of ions identified in each SSA and SDA ions populations. Present results show that the ions energization is quite efficient only during a fraction (approximately 1/3) of the self-reformation cycle since the average kinetic energy increases but saturates almost simultaneously for both populations around time $\tilde{t} = 1790$. This time corresponds to that for which the time variation of the relative percentage of SSA and SDA ions separate each other (Figure 5c). Previous works [*Lembège and Savoini*, 1992; *Yang et al.*, 2009] have shown that the density of reflected ions varies in time with a period equal to that of the shock front self-reformation cycle. In addition, present Figure 5 demonstrates that, within this cycle, the energization efficiency is not shared equally by SDA and SSA ions but strongly differs for each reflected ions population.

4.2. Ion Shell Distribution (Pickup Ions)

[26] Secondly, we investigate the pickup ion spectrum for a long time range covering at least five self-reformation cycles and where PIs interact with a continously time-evolving shock. Test particles are distributed evenly within a wide region $4637 < \tilde{X}_i < 6007$ at a chosen starting time $\tilde{t} = 628$. At that time, the shock front is released and propagates with its instantaneous shock velocity (instead of its time-averaged velocity measured at the ramp), and the simulation continues until time $\tilde{t} = 1856$. Figure 6a shows the spectra of PIs for shell distributions with different initial shell radii ($\tilde{V}_{shell} = 5$, 10, 28 and $48\tilde{V}_{thix,y,z}$). The time averaged energy spectrum of PIs is calculated from upstream ($\tilde{X}_{ramp} + 300$) to downstream ($\tilde{X}_{ramp} - 600$) at the ending time $\tilde{t} = 1856$ during the 5th cycle. By that time, all upstream particles have interacted with the shock front over a long time range ($\sim 1\tilde{\tau}_{ci}$ at least) and are located downstream. Figure 6a shows the corresponding downstream PI's spectra calculated from the ramp to far downstream ($\tilde{X}_{ramp} - 600$) in the upstream frame. The comparison with results obtained in the fixed shock regime (section 3) leads to the following statements:

[27] 1. The self-consistent nonstationary effects do have two striking features. First, the self-reformation largely increases the contribution of SSA ions in the total spectrum whatever the $\tilde{V}_{shell}$ value is (Figure 6a); this is particularly noticeable for small $\tilde{V}_{shell}$ cases where SSA ions have been absent or rare for a fixed shock profiles (first and second rows of Figure 4). However, this reinforcement of SSA ions is only relative since SDA ions are clearly dominant in most cases. Second, the self-reformation sustains quite well the formation of monoenergetic SSA PIs for high $\tilde{V}_{shell}$ case (fourth panel of Figure 6a). This means that such a population mainly evidenced for the fixed shock profile I (fourth

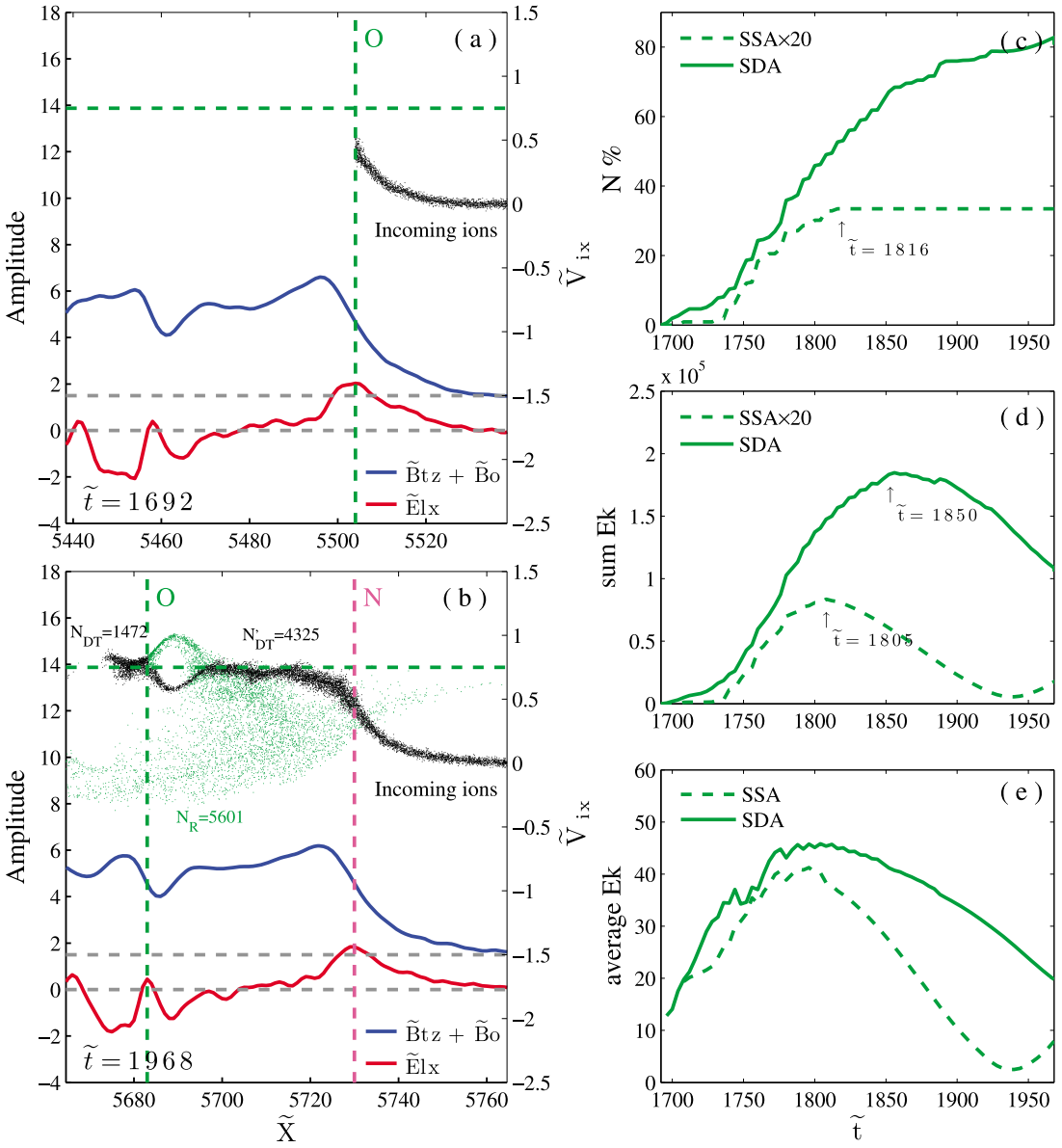

Figure 5. Shock profiles and ions phase space plot ($\tilde{V}_{xi} - \tilde{X}_i$) at the (a) beginning time $\tilde{t}$ = 1692 and (b) ending time $\tilde{t}$ = 1968 of the fifth self-reformation cycle. SDA and SSA ions reflected by the old ramp during this cycle are denoted by green dots; directly transmitted and incoming ions are in black. The new ramp ("N") and old ramp ("O") are marked by magenta and green vertical dashed lines, respectively. Horizontal dashed lines indicate the instantaneous shock velocity (green), the upstream ambient magnetic field strength (1.5), and the reference $\tilde{E}_{lx}$ = 0 value, respectively. (c) The percentage, (d) the total kinetic energy, and (e) the average kinetic energy of SDA (solid) and SSA (dashed) ions versus time within the same fifth reformation cycle (1692 < $\tilde{t}$ < 1968).

panel of Figure 4a) still persists in presence of nonstationary effects.

[28] 2. The energy spectrum of each population (and the resulting total spectrum) shrinks as $\tilde{V}_{shell}$ increases. This shrinking is particularly pronounced for SSA ions, but is larger for SDA and DT ions. It is also more pronounced with respect to the fixed shock profiles cases (Figure 4).

[29] Figure 6b shows the corresponding downstream PI's spectra calculated from the ramp to far downstream ($\tilde{X}_{ramp}$ − 600) and measured in the shock rest frame. The use of this frame allows to stress more clearly some important features and facilitates the comparison with previous works using the same frame. The total spectra (blue curve) exhibit some slopes variation (shoulder) at locations marked by downward arrows B and C. Let us note that B and C also correspond to the energy value where the contribution of SDA and DT ions separate each other (at least for low $\tilde{V}_{shell}$ cases), and where the contribution of SSA ions is almost zero (SDA only becomes dominant). Present results stress the following features:

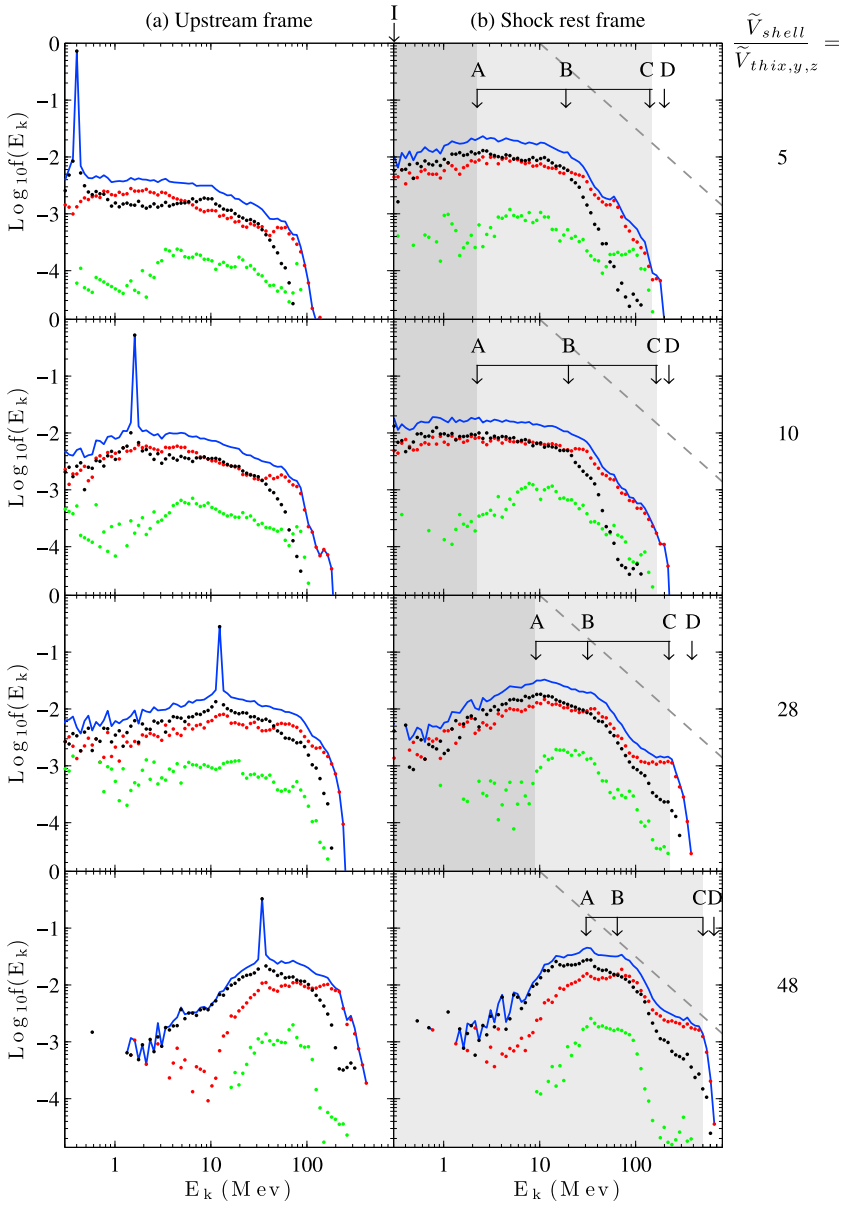

Figure 6. Energy spectra of PIs defined for different initial shell velocities $\tilde{V}_{shell} = 5$, 10, 28 and $48\tilde{V}_{thix,y,z}$ and obtained for a continuously time-varying nonstationary shock. Definition of dots are similar to those of Figure 4. (a) Energy spectra are measured from upstream ($\tilde{X}_{ramp} + 300$) to downstream ($\tilde{X}_{ramp} - 600$) in the upstream frame (i.e., present simulation). (b) Corresponding downstream energy spectra measured from the ramp to downstream ($\tilde{X}_{ramp} - 600$) in the shock rest frame. The $E_k^{-1.5}$ power law is shown for reference. Low, middle, and high energy ranges of the total spectra are denoted by different gray scale highlight.

[30] 1. As $\tilde{V}_{shell}$ increases, both B and C locations shift to higher energy.

[31] 2. Low, middle, and high energy ranges of the total energy spectra (blue curve) are defined by ranges (I–A), (A–C), and (C–D), respectively, where the arrow A corresponds to the energy value where the total density is maximum, the arrow I to the initial kinetic energy and the arrow D to the high energy cutoff. For convenience of presentation, these ranges are denoted by different gray scale highlights, in order to compare with results obtained in previous papers [*Zank et al.*, 1996; *Burrows et al.*, 2009]. A dashed line representing a $E_k^{-1.5}$ power law has been plotted for reference over the computed spectrum within each panel of Figure 5b. Present results show that two slopes may be defined in the middle energy range within A–B and B–C ranges in particular for low $\tilde{V}_{shell}$ cases (first and second panels of Figure 6b). But, these slopes reduce almost to one which corresponds to that defined within the A–B range for high $\tilde{V}_{shell}$ cases (third and fourth panels of Figure 6b), since the middle energy range strongly shrinks as $\tilde{V}_{shell}$ increases. In order to illustrate the

slopes variation with $\tilde{V}_{shell}$, we concentrate herein on that defined within A–B range used as a reference. The important feature is that the total energy spectrum follows a power law in this range, whose index varies from 2.3 to 2.2, 1.5 and 1.52 as $\tilde{V}_{shell}$ increases (Figure 6b). Let us remind that the highest value $\tilde{V}_{shell}$ (=48$\tilde{V}_{thix,y,z}$ = 0.81) almost corresponds to the shock velocity ($\tilde{V}_{shock}$ = 0.83). Then, a good agreement is reached with the power law $E_k^{-1.5}$ obtained by *Burrows et al.* [2009] for similar $\tilde{V}_{shell}$ case (equal to the shock velocity). However, a full agreement is not obtained yet, since *Burrows et al.* [2009] found that the key acceleration process is SSA, while present results show the dominance of SDA process in comparable (middle) energy range. Further analysis is still under active investigation to clarify this point.

[32] 3. Within the middle energy range (A–C), the contribution of the different ions populations to the total spectrum strongly varies according to the $\tilde{V}_{shell}$ case. DT and SSA PIs alternately dominate for low $\tilde{V}_{shell}$ cases (the sets of black and green dots cross each other in first and second panels of Figure 6b) while SSA PI's contribution becomes poor for high $\tilde{V}_{shell}$ case. Moreover, for high $\tilde{V}_{shell}$ cases (third and fourth panels of Figure 6b), DT and SDA ions dominate in range (A–B), but SDA ions dominate in range (B–C) for Figure 6b (third and fourth panels). For low $\tilde{V}_{shell}$ case (Figure 6b, first panel), SDA and SSA ions have a comparable contribution around arrow C; within the frame of the present analysis, this represents the only case of a noticeable contribution of SSA to the formation of energetic PIs.

5. Discussions and Conclusions

[33] In this paper, we have used test particle simulations where the fields of a nonstationary shock are issued from a 1-D PIC self-consistent simulation in order to analyze the effects of the shock front nonstationarity and of a varying initial energy of the shell distribution on the dynamics and the resulting energy spectrum of PI's ions at a supercritical perpendicular shock. Herein, the front nonstationarity corresponds to the shock self-reformation due to the accumulation of reflected ions, as evidenced in previous PIC and hybrid simulations. We have investigated in details the contributions of each energization process (SDA, SSA and DT ions) to the total energy spectrum. Three comparative approaches have been followed and are based on (1) fixed shock profiles chosen at different times of a given self-reformation cycle and (2) a shock profile continuously time-evolving over five reformation cycles (nonstationary shock). The first case allows the impact of a developing foot and of the self-consistent variations of ramp fields to be analyzed gradually (spatial scales and amplitudes) on the energy spectra. The second case allows the impact of self-consistent nonstationarity effects to be analyzed in order to approach more realistic conditions. Main results can be summarized as follows:

[34] 1. According to the results obtained at fixed shock profiles (first case), SSA ions only appear for relatively large shell cases whatever the shock profile. In addition, the maximum density of SDA and SSA ions in the middle energy range of the spectrum decreases as the shock front width (including foot and ramp) increases from profiles I to II. This decrease is more clearly evidenced between profiles I and II.

[35] 2. SSA and SDA still work together at nonstationary shocks (second case) but their relative contribution to the total spectrum strongly varies versus the initial shell radius and the energy range under consideration within this spectrum.

[36] 3. A power law type $E_k^{-1.5}$ is recovered in the middle energy range of the total spectrum for high $\tilde{V}_{shell}$ values (in particular as $\tilde{V}_{shell}$ value is around the shock velocity) in agreement with previous works. However, this agreement is only partial since SDA, and not SSA, process reveals to be the most efficient mechanism in the formation of energetic PIs. The contribution of SSA PIs is comparatively weak. In all cases, SDA ions dominate in the high energy range.

[37] Moreover, a separate analysis based on an upstream Maxwellian distribution has shown that, while the density of reflected ions (SDA and SSA ions mixed) varies in time with a period equal to that of the shock front self-reformation cycle, the energization efficiency within this cycle strongly differs for SDA and SSA ions. In addition, the SSA process is quite efficient as the width of the shock front is very narrow [*Lever et al.*, 2001]. The self-reformation allows the shock front to reach such a very narrow width (the narrow ramp covering a few electron inertial lengths) and was expected to be in favor of dominant SSA process. However, the 1-D PIC simulation by *Scholer et al.* [2003] has stated that only part of the potential drop at the front occurs for relatively short times over a few electron inertial lengths and that coherent shock surfing is not an efficient acceleration mechanism for pickup ions at the low β heliospheric termination shock. Furthermore, this work did not compare the efficiency of SDA and SSA process for a given shock. Although present results do not strictly apply to the terminal shock (which has strong PI's percentage), these illustrate more precisely that energetic SSA ions are only generated within one third of each reformation cycle. This feature can be related to the strong decrease of the cross-shock potential at the ramp taking place within the remaining two thirds stage of the cycle. Present results confirm quantitatively the argument on low contribution of SSA ions at reforming perpendicular shocks proposed by *Scholer et al.* [2003].

[38] Our present results are based on 1-D PIC simulations of perpendicular shock where the front nonstationary is supported by the self-reformation mainly driven by the background protons only. This approach is motivated by the fact that this process has been shown to be quite robust and persist in monodimensional and multidimensional PIC and hybrid simulations for perpendicular and quasi-perpendicular shocks, and for low/high mass ratio and ω_{pe}/Ω_{ce} ratio values. The most simple configuration (perpendicular shock) and low mass ratio have been chosen in order to avoid any pollution by whistler waves emission and presence of microstabilities. The impact of this self-reformation on PIs has been analyzed by considering the PIs as test particles. This approach applies to cases (such as CIR-associated shocks and CME-driven shocks beyond a few tens of AU) where the PI's percentage is not high enough to affect the microstructures of the shock front and its nonstationary dynamics (self-reformation); no feedback effect of PIs takes place on the shock itself. In particular, present results cannot apply to the termination shock where the PI's density is estimated as very high (about 20–25%). Self-consistent investigation of the termination shock including both particle species (background ions and PIs) will be necessary and is under active investigation.

[39] **Acknowledgments.** This work has been performed while one of the authors (Z.Y.) was staying in LATMOS (France), which is thanked for its hospitality and access to computing facilities. This research work was partly supported by the National Science Foundation of China grants 40931053, 40725013, Chinese Academy of Sciences KJCX2-YW-N28, and the State Scholarship Fund of China Scholarship Council 2009102786. The initial one-dimensional PIC simulations have been performed on the supercomputer of IDRIS center located at Orsay (near Paris).

[41] Philippa Browning thanks the reviewers for their assistance in evaluating this paper.

References

Axford, W. I., E. Lee, and G. Skadron (1977), The acceleration of cosmic rays by shock waves, paper presented at 15th International Cosmic Ray Conference, Bulgarian Acad. of Sci., Plovdiv, Bulgaria, 13–26 Aug.

Begelman, M., and J. G. Kirk (1990), Shock-drift particle acceleration in superluminal shocks: A model for hot spots in extragalactic radio sources, *Astrophys. J.*, *353*, 66–80.

Bell, A. R. (1978a), The acceleration of cosmic rays in shock fronts. I, *Mon. Not. R. Astrophys. Soc.*, *182*, 147–156.

Bell, A. R. (1978b), The acceleration of cosmic rays in shock fronts. II, *Mon. Not. R. Astrophys. Soc.*, *182*, 443–455.

Biskamp, D., and H. Welter (1972), Ion heating in high-Mach-number, oblique, collisionless shock waves, *Phys. Rev. Lett.*, *28*, 410–413.

Blandford, R. D., and D. Eichler (1987), Particle acceleration at astrophysical shocks: A theory of cosmic ray origin, *Phys. Rep.*, *154*, 1–75.

Blandford, R. D., and J. P. Ostriker (1978), Particle acceleration by astrophysical shocks, *Astrophys. J.*, *221*, L29–L32.

Burgess, D., W. P. Wilkinson, and S. J. Schwartz (1989), Ion distribution and thermalization at perpendicular and quasi-perpendicular supercritical collisionless shocks, *J. Geophys. Res.*, *94*(A7), 8783–8792.

Burrows, R. H., G. P. Zank, and G. M. Webb (2009), Termination shock surfing, *AIP Conf. Proc.*, *1183*, 47–56.

Chalov, S. V. (2001), Shock drift acceleration of pickup protons at corotating interaction regions, *J. Geophys. Res.*, *106*(A9), 18,667–18,675.

Chapman, S. C., R. E. Lee, and R. O. Dendy (2005), Perpendicular shock reformation and ion acceleration, *Space Sci. Rev.*, *121*, 5–19.

Decker, R. B. (1988), Computer modeling of test particle acceleration at oblique shocks, *Space Sci. Rev.*, *48*, 195–262.

Decker, R. B., and L. Vlahos (1985), Shock drift acceleration in the presence of waves, *J. Geophys. Res.*, *90*(A1), 47–56.

Giacalone, J. (2004), Large-scale hybrid simulations of particle acceleration at a parallel shock, *Astrophys. J.*, *609*, 452–458.

Hada, T., M. Oonishi, B. Lembège, and P. Savoini (2003), Shock front nonstationarity of supercritical perpendicular shocks, *J. Geophys. Res.*, *108*(A6), 1233, doi:10.1029/2002JA009339.

Hellinger, P., P. Travnicek, and H. Matsumoto, (2002), Reformation of perpendicular shocks: Hybrid simulations, *Geophys. Res. Lett.*, *29*(24), 2234, doi:10.1029/2002GL015915.

Hellinger, P., P. Travnicek, B. Lembège, and P. Savoini, (2007), Emission of nonlinear whistler waves at the front of perpendicular supercritical shocks: Hybrid versus full particle simulations, *Geophys. Res. Lett.*, *34*, L14109, doi:10.1029/2007GL030239.

Hudson, P. D. (1965), Reflection of charged particles by plasma shocks, *Mon. Not. R. Astron. Soc.*, *131*, 23–50.

Katsouleas, T., and J. M. Dawson (1983), Unlimited electron acceleration in laser-driven plasma waves, *Phys. Rev. Lett.*, *51*, 392–395.

Krymsky, G. F. (1977), A regular mechanism for accelerating charged particles at the shock front, *Dokl. Akad. Nauk SSSR*, *234*, 1306–1308.

Lee, M. A. (1983), Coupled hydromagnetic wave excitation and ion acceleration at interplanetary traveling shocks, *J. Geophys. Res.*, *88*(A8), 6109–6119.

Lee, M. A. (1999), The injection, acceleration, and dynamical influence of interstellar PI's at the solar wind termination shock, *Astrophys. Space Sci.*, *264*, 497–508.

Lee, M. A., V. D. Shapiro, and R. Z. Sagdeev (1996), Pickup ion energization by shock surfing, *J. Geophys. Res.*, *101*(A3), 4777–4789.

Lee, R. E., S. C. Chapman, and R. O. Dendy (2004), Numerical simulations of local shock reformation and ion acceleration in supernova remnants, *Astrophys. J.*, *604*, 187–195.

Lee, R. E., S. C. Chapman, and R. O. Dendy (2005a), Ion acceleration processes at reforming collisionless shocks, *Phys. Plasmas*, *12*, 012901, doi:10.1063/1.1812536.

Lee, R. E., S. C. Chapman, and R. O. Dendy (2005b), Reforming perpendicular shocks in the presence of pickup protons: Initial ion acceleration, *Ann. Geophys.*, *23*, 643–650.

Lembège, B. (1989), Numerical simulations of collisionless shocks, in *Physical Processes in Hot Cosmic Plasmas*, *NATO ASI Ser. C, Math. and Phys. Sci.*, vol. 301, edited by W. Brinkman, A. C. Fabian, and F. Giovannelli, pp. 81–139, Kluwer Acad., Boston, Mass.

Lembège, B., and J. M. Dawson (1987), Self-consistent study of a perpendicular collisionless and nonresistive shock, *Phys. Fluids*, *30*, 1767–1788.

Lembège, B., and P. Savoini (1992), Nonstationarity of a two-dimensional quasiperpendicular supercritical collisionless shock by self-reformation, *Phys. Fluids B*, *4*, 3533–3544.

Lembège, B., J. Giacalone, M. Scholer, T. Hada, M. Hoshino, V. Krasnoselskikh, H. Kucharek, P. Savoini, and T. Terasawa (2004), Selected problems in collisionless-shock physics, *Space Sci. Rev.*, *110*, 161–226.

Lembège, B., P. Savoini, P. Hellinger, and P. Travnicek (2009), Nonstationarity of a two-dimensional perpendicular shock: Competing mechanisms, *J. Geophys. Res.*, *114*, A03217, doi:10.1029/2008JA013618.

Lever, E. L., K. B. Quest, and V. D. Shapiro (2001), Shock surfing vs. shock drift acceleration, *Geophys. Res. Lett.*, *28*(7), 1367–1370.

Li, G., G. P. Zank, and W. K. M. Rice (2003), Energetic particle acceleration and transport at coronal mass ejection drive shocks, *J. Geophys. Res.*, *108*(A2), 1082, doi:10.1029/2002JA009666.

Liewer, P., B. Goldstein, and N. Omidi (1993), Hybrid simulations of the effects of interstellar pickup hydrogen on the solar wind termination shock, *J. Geophys. Res.*, *98*(A9), 15,211–15,220.

Lobzin, V. V., V. V. Krasnoselskikh, J.-M. Bosqued, J.-L. Pincon, S. J. Schwartz, and M. Dunlop (2007), Nonstationarity and reformation of high-Mach-number quasiperpendicular shocks: Cluster observations, *Geophys. Res. Lett.*, *34*, L05107, doi:10.1029/2006GL029095.

Malkov, M. A., and L. O. Drury (2001), Nonlinear theory of diffusive acceleration of particles by shock waves, *Rep. Prog. Phys.*, *64*, 429–481.

Matsukiyo, S., M. Scholer, and D. Burgess (2007), Pickup protons at quasi-perpendicular shocks: Full particle electrodynamic simulations, *Ann. Geophys.*, *25*, 283–291.

Mazelle, C., B. Lembège, A. Morgenthaler, K. Meziane, T. S. Horbury, V. Genot, E. A. Lucek, and I. Dandouras (2009), Self-reformation of the quasi-perpendicular shock: Cluster observations, *AIP Conf. Proc.*, *1216*, 471–474.

Morse, D. L., W. W. Destler, and P. L. Auer (1972), Nonstationary behavior of collisionless shocks, *Phys. Rev. Lett.*, *28*, 13–16.

Muschietti, L., and B. Lembège (2006), Electron cyclotron microinstability in the foot of a perpendicular shock: A self-consistent PIC simulation, *Adv. Space Res.*, *37*, 483–493.

Nishimura, K., H. Matsumoto, H. Kojima, and S. P. Gary (2003), Particle simulation of re-formation at collisionless perpendicular shocks: Coherent behavior of reflected ions, *J. Geophys. Res.*, *108*(A5), 1182, doi:10.1029/2002JA009671.

Sagdeev, R. Z. (1966), Cooperative phenomena and shock waves in collisionless plasmas, *Rev. Plasma Phys.*, *4*, 23–91.

Schmitz, H., S. C. Chapman, and R. O. Dendy (2002), Electron preacceleration mechanisms in the foot region of high Alfvénic Mach number shocks, *Astrophys. J.*, *579*, 327–336.

Scholer, M., and S. Matsukiyo (2004), Nonstationarity of quasi-perpendicular shocks: A comparison of full particle simulations with different ion to electron mass ratio, *Ann. Geophys.*, *22*, 2345–2353.

Scholer, M., I. Shinohara, and S. Matsukiyo (2003), Quasi-perpendicular shocks: Length scale of the cross-shock potential shock reformation, and implication for shock surfing, *J. Geophys. Res.*, *108*(A1), 1014, doi:10.1029/2002JA009515.

Shapiro, V. D., and D. Ucer (2003), Shock surfing acceleration, *Planet. Space Sci.*, *51*, 665–680.

Shimada, N., and M. Hoshino (2000), Strong electron acceleration at high Mach number shock waves: Simulation study of electron dynamics, *Astrophys. J.*, *543*, L67–L71.

Shinohara, I., M. Fujimoto, R. Takaki, and T. Inari (2011), A three-dimensional particle-in-cell simulation of quasi-perpendicular shock on Fujitsu FX-1 cluster, *IEEE Trans. Plasma Sci.*, *39*, 1173–1179.

Tidmann, D., and N. Krall (1971), *Shock Waves in Collisionless Plasmas*, Wiley-Interscience, New York.

Tsurutani, B. T., and R. G. Stone (Eds.) (1985), *Collisionless Shocks in the Heliosphere: Reviews of Current Research*, *Geophys. Monogr. Ser.*, vol. 303, AGU, Washington, D. C.

Vasyliunas, V. M., and G. L. Siscoe (1976), On the flux and the energy spectrum of interstellar ions in the solar system, *J. Geophys. Res.*, *81*(7), 1247–1252.

Webb, G. M., W. I. Axford, and T. Terasawa (1983), On the drift mechanism for energetic charged particles at shocks, *Astrophys. J.*, *270*, 537–553.

Webb, G. M., G. P. Zank, M. Ko, and D. J. Donohue (1995), Multidimensional Green's functions and the statistics of diffusive shock acceleration, *Astrophys. J.*, *453*, 178–206.

Wu, P., D. Winske, S. P. Gary, N. A. Schwadron, and M. A. Lee (2009), Energy dissipation and ion heating at the heliospheric termination shock, *J. Geophys. Res.*, *114*, A08103, doi:10.1029/2009JA014240.

Yang, Z. W., Q. M. Lu, B. Lembège, and S. Wang (2009), Shock front nonstationarity and ion acceleration in supercritical perpendicular shocks, *J. Geophys. Res.*, *114*, A03111, doi:10.1029/2008JA013785.

Zank, G. P., H. L. Pauls, I. H. Cairns, and G. M. Webb (1996), Interstellar pickup ions and quasi-perpendicular shocks: Implications for the termination shock and interplanetary shocks, *J. Geophys. Res.*, *101*(A1), 457–477.

Zank, G. P., G. Li, V. Florinski, Q. Hu, D. Lario, and C. W. Smith (2006), Particle acceleration at perpendicular shock waves: Model and observations, *J. Geophys. Res.*, *111*, A06108, doi:10.1029/2005JA011524.

Zank, G. P., J. Heerikhuisen, N. V. Pogorelov, R. Burrows, and D. McComas (2010), Microstructure of the heliospheric termination shock: Implication for energetic neutral atom observations, *Astrophys. J.*, *708*, 1092–1106.

B. Lembège, LATMOS-UVSQ-IPSL-CNRS, Guyancourt F-78280, France. (bertrand.lembege@latmos.ipsl.fr)

Q. M. Lu and Z. W. Yang, CAS Key Laboratory of Basic Plasma Physics, School of Earth and Space Sciences, University of Science and Technology of China, Hefei, Anhui 230026, China. (qmlu@ustc.edu.cn)